Scrutinizing intrinsic oxygen reduction reaction activity of a Fe–N–C catalyst via scanning electrochemical cell microscopy

Ndrina Limani, Emmanuel Batsa Tetteh, Moonjoo Kim, Thomas Quast, Emmanuel Scorsone, Bruno Jousselme, Wolfgang Schuhmann, Renaud Cornut

ChemElectroChem

Research Article
doi.org/10.1002/celc.202201095

Chemistry Europe
European Chemical Societies Publishing

www.chemelectrochem.org

Scrutinizing Intrinsic Oxygen Reduction Reaction Activity of a Fe–N–C Catalyst via Scanning Electrochemical Cell Microscopy

Ndrina Limani,[a, b] Emmanuel Batsa Tetteh,[b] Moonjoo Kim,[b, c] Thomas Quast,[b] Emmanuel Scorsone,[d] Bruno Jousselme,[a] Wolfgang Schuhmann,*[b] and Renaud Cornut*[a]

Carbon-based nanomaterials are renowned for their exceptional properties, making them propitious candidates for oxygen reduction reaction (ORR) electrocatalysis. However, their intrinsic activity is often challenging to investigate unambiguously with conventional methodologies due to the inherent complexities of such systems and the material itself. Zooming into the material and gaining electrochemical information with high resolution is a way to get rid of many experimental factors that influence the catalytic activity in macro-scale measurements. Herein, we employ nano-scale scanning electrochemical cell microscopy (SECCM) to investigate individual catalyst agglomerates with and without Nafion content. The intrinsic ORR activity of the catalyst was unravelled by using a unique approach of normalizing the data of all measured points by their distinctive electrochemical surface area (ECSA). When coupling with scanning electron microscopy (SEM), the structure and morphology of the catalytically active agglomerates were visualized.

Introduction

The fuel cell commercialization is currently on hold, mainly due to the complicated cathode reaction (ORR), the scarce state-of-the-art Pt electrocatalysts needed for it and the enormous challenges in developing, understanding and characterizing Pt-free materials.[1,2] Carbon nanotube-based materials are distinguished as auspicious non-precious electrocatalysts owing to their high conductivity, surface area, stability and their accessibility, making the research towards their development contemporary.[3] Synthesizing novel catalytic materials is crucial in the field, yet their unambiguous electrochemical characterization of ORR activity is just as important. In conventional ORR investigation methods such as rotating disc electrode (RDE), there are many experimental factors to take into account, such as catalyst thickness,[4] porosity, Nafion content, electrochemical reactions of the surrounding environment in the electrolyte, mass transport issues etc.,[5] making the extraction of intrinsic activity quite complicated or even impossible.

Scanning probe microscopy (SPM) techniques have gained attention lately for electrocatalytic activity studies due to the many advantages they provide, mainly the small probes which allow high spatial resolutions and higher mass transfers.[6–8] Scanning electrochemical microscopy (SECM)[9,10] is one of the SPM techniques which is being used increasingly by the community to evaluate ORR activity, especially after the invention of redox competition (RC) mode.[11] This technique allows the extraction of crucial data about the catalysts' activity and selectivity mainly with a ~10–25 μm Pt ultra-microelectrode (UME).[6] This resolution is limited to a few micrometers and the electrochemical information represents the global averaged activity of many agglomerates in a deposit. Therefore, one can see a rather homogeneous distribution of activity in a typical SECM map.[12,13]

Being able to zoom into tiny structures of the material and performing single-entity electrochemistry could in principle mitigate such obstacles. One of the SPM techniques which allows high-resolution single-entity electrochemical measurements is scanning electrochemical cell microscopy (SECCM),[14,15] a technique whose principle consists in scanning the sample with an easy fabricable electrolyte-filled pipette with a reference counter electrode (RCE) inside.[16] At the end of the pipette, a droplet is generated which will give a feedback current when in contact with the sample, in which case electrochemistry can be performed in that specific small area without any influence of the surrounding.[17] The configuration

[a] Dr. N. Limani, Dr. B. Jousselme, Dr. R. Cornut
Universite Paris-Saclay
CEA, CNRS, NIMBE, LICSEN
Gif-sur-Yvette, 91191 (France)
E-mail: renaud.cornut@cea.fr
[b] Dr. N. Limani, Dr. E. Batsa Tetteh, M. Kim, Dr. T. Quast, Prof. Dr. W. Schuhmann
Analytical Chemistry-Center for Electrochemical Sciences (CES)
Faculty of Chemistry and Biochemistry
Ruhr University Bochum
Universitätsstraße 150, Bochum (Germany)
E-mail: wolfgang.schuhmann@rub.de
[c] M. Kim
Department of Chemistry
Seoul National University
Seoul 08826 (Republic of Korea)
[d] Dr. E. Scorsone
Université Paris-Saclay
CEA, List
91120, Palaiseau (France)

Supporting information for this article is available on the WWW under https://doi.org/10.1002/celc.202201095

of SECCM allows high oxygen mass transport considering that O_2 is provided by the liquid-air interface of the meniscus, in addition to the O_2 transported through the barrel,[18] making it a promising technique for ORR investigation. The usage of nano-sized pipettes and a small hopping distance allows one to perform hundreds to thousands of individual measurements within one sample with ultra-high resolution, at a time scale of only a few hours.[19] To put it into perspective, what we would see as one pixel in a SECM map, we could discern as thousands of pixels in a SECCM map, which can further be coupled with SEM to correlate the activity with the morphology of the studied entities (Figure 1b). There are however fewer reported works regarding ORR investigation with SECCM, for example, Tetteh et al.[20] studied ORR of a complex solid solution (CSS) revealing heterogeneities in activity when scanning with a nano-sized pipette. Moreover, Byers et al.[21] studied single-walled carbon nanotubes (SWCNT) with high-resolution SECCM revealing that the SWCNT alone are active for ORR and Mariano et al.[22] investigated the ORR activity of a metal-organic framework (MOF) via SECCM.

Even in small entities investigated by SECCM, the porosity and surface area of catalyst agglomerates can influence the activity, generating the necessity of taking into account the surface area for unambiguous conclusions. Herein, we investigate the ORR activity of a multi-walled carbon nanotube-based material modified with Fe and N (Fe–N-MWCNT) using SECCM. By normalizing thousands of individual measurements by their unique electrochemical surface area (ECSA), we unravel the intrinsic activity of the catalyst uninfluenced by their area, in agglomerates with and without Nafion content. Moreover, through coupling with scanning electron microscopy (SEM), we were able to scrutinize the morphology of the active catalyst spots.

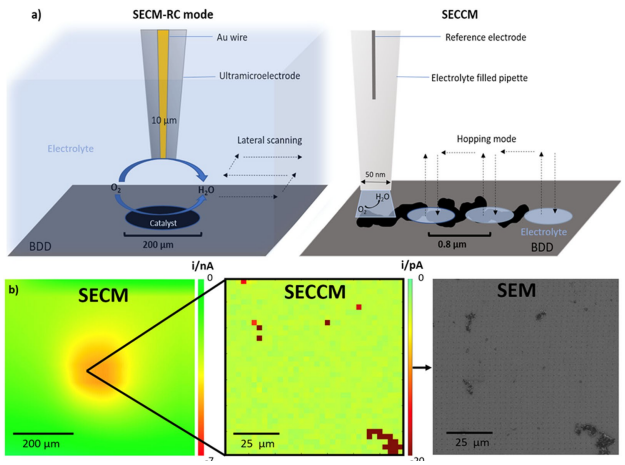

Figure 1. (a) Scheme representing the principle of SECM and SECCM techniques, (b) scheme showing an example of an SECM map acquired with 10 µm Au UME in RC mode (left) and how one pixel of the SECM map can be discerned as thousands of pixels with an SECCM map to differentiate between different catalyst agglomerates (middle), followed by an SEM image of the SECCM scanned area for additional morphology information (right). Note this is only an illustration, as SECM and SECCM maps do not correspond to the same deposit.

Results and Discussion

In this work, SECCM was employed to investigate individual agglomerates of a non-precious Fe–N-MWCNT catalyst. The catalyst ink was drop-cast on a flat boron-doped diamond (BDD) substrate, which is inert and hence does not contribute to the measured currents due to its high overpotential for oxygen reduction.[23] Subsequently, the sample was analyzed with SECCM using a ~150 nm pipette. The SECCM measurement spanned an area of 40×40 µm^2, with a hopping distance of 0.8 µm leading to 51×51 landing points thus 2601 individual linear sweep voltammogram (LSV) measurements. Throughout the scan, the z-position of the capillary was monitored, generating a topography map as shown in Figure S1a where the highest landing point corresponds to 730 nm for spot 1, followed by 666 nm and 380 nm for spot 2 and 3 respectively.

The LSVs recorded for all landing spots were translated into activity maps and the map at 0.56 V vs RHE is presented in Figure S1b, showing a homogeneous map with almost no current at such overpotentials. On the other hand, the activity map at 0 V vs RHE in Figure 2a shows an inert BDD substrate covered with active catalyst spots which are easily distinguished by their higher currents. The size of the catalyst studied here (~11 nm, Figure S2) is significantly smaller than the size of the pipette (~150 nm), therefore the high current areas could correspond to small agglomerates. When analyzing the LSVs corresponding to designated pixels in the activity map (Figure 2b), spot 2 shows a significantly higher current (170 pA) compared to spot 1 and 3 with <20 pA. Nevertheless, something that has to be taken into account when making comparisons within different spots is that their ECSA could be different, meaning that a simple high current-high activity conclusion could be misleading. This ambiguity was overcome by normalizing the currents with the electrochemical surface area (ECSA).[24] The latter was derived from the double-layer capacitance (C_{dl}) and specific capacitance (C_s) according to the expression ECSA = C_{dl}/C_s. Cyclic voltammograms (CVs) were performed at different scan rates in a non-faradaic potential region (0.906 V–0.956 V vs RHE) (Figure S3), and from the slope of current vs scan rate we extracted C_{dl}. The coefficient of determination (R^2) for the fits of each pixel (landing point) is

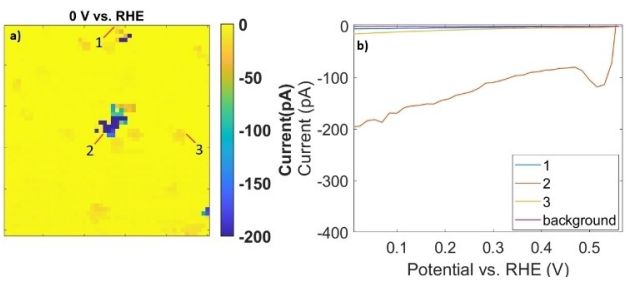

Figure 2. (a) Activity map showing the current in pA at 0 V vs RHE with the investigated agglomerates designated as 1,2,3. (b) LSVs showing the current (pA) vs E vs RHE for the designated pixels in the map. Data correspond to the scan with 40×40 µm^2 area, 0.8 µm hopping distance, acquired with a ~150 nm pipette filled with 0.05 M H_2SO_4. Catalyst agglomerates contain Nafion.

used to verify the quality of the fit and the R^2 map with the values for the studied pixels are shown in Figure S4 and Table S1 respectively. The spots with an $R^2 \geq 0.97$ were chosen for the study. The C_{dl} map and its values for all designated spots are shown in Figure 3 and Table S1 respectively. We divided the C_{dl} with a value of C_s (0.0415 F cm^{-2}) reported for carbon nanotubes (CNT),[25] hence acquiring the ECSA in cm^2 and using it to normalize the current values at each measured spot. The ECSA normalized LSVs in Figure 4b show more similar current densities between −200 and −300 mA cm^{-2}, rather than the disparate currents in Figure 2b. When analyzing the shape of the LSVs, one can see that they do not exhibit diffusion-limited currents (i_L) due to the high O_2 mass transport into the small droplet, in which case the i_L is shifted to more cathodic potentials.[18,20] For the same reason, the observed current values are orders of magnitude higher than one would foresee.[22,26]

Moreover, while the LSVs correspond to specifically designated spots, the activity map gives us an overall idea of the activity during the whole scan. After normalizing the current with ECSA, the activity map exhibits higher current densities throughout the lower half of the substrate (Figure 4a) which is vastly different from the non-normalized map. The upper part of the scan also shows higher current densities, apparent on the LSV of the background (−60 mA cm^{-2}). To get further insight into this, we subsequently analyzed the SECCM scanned area of the sample with SEM as shown in Figure S5. Even though one would anticipate seeing small spherical landing traces of the meniscus, the electrolyte was in fact spread onto the substrate and thus flooded the lower half of the scan, with no individual landing spots being visible. This flooded area matches the higher activity in the same region in Figure 4a. It should be noted that all data were normalized by using a C_s corresponding to CNT (0.0415 F cm^{-2}), while the C_s value for the BDD substrate is typically only about 3 μF cm^{-2}.[27] This might have led to an ECSA lower than predicted, hence leading to a higher current density in the background (BDD). To confirm this, the ECSA normalized activity map considering the BDD C_s is shown in Figure S6 with almost no current, where of course, herein the activity of the catalyst spots does not appear in the map. It is evident that only by ECSA normalization and usage of the appropriate C_s, one can have an idea about the quality of the experiment with the intrinsic activity of the catalyst and the inertness of the BDD substrate in the applied potential region.

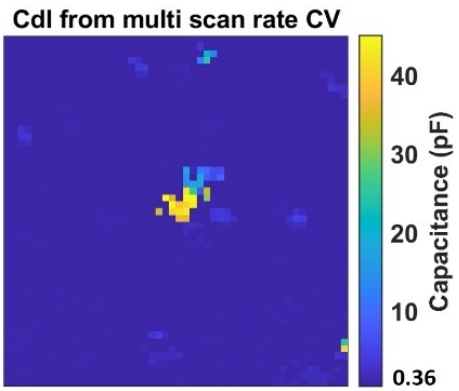

Figure 3. Double layer capacitance C_{dl} acquired from the slope of current vs scan rate, data corresponds to the scan with 40×40 μm^2 area, 0.8 μm hopping distance, acquired with a ~150 nm pipette filled with 0.05 M H_2SO_4. Catalyst agglomerates contain Nafion.

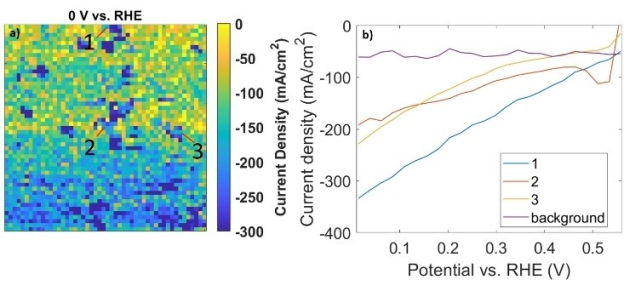

Figure 4. (a) Activity map normalized by ECSA showing the current density in mA cm^{-2} at 0 V vs RHE with the investigated agglomerates designated as 1,2,3. (b) Corresponding LSVs for the designated pixels in the normalized activity map, showing current density (mA cm^{-2}) vs E vs RHE. Data corresponds to the scan with 40×40 μm^2 area, 0.8 μm hopping distance, acquired with a ~150 nm pipette filled with 0.05 M H_2SO_4. Catalyst agglomerates contain Nafion.

We zoomed into the individual catalyst spots with SEM (Figure S7) in order to have an insight into the morphology of the catalyst. The structure of the material was undetermined in most of the spots, with the exception of spot 2 where one can recognize the carbon nanotubes more clearly. Considering that the SEM images reveal smooth and liquid-like features of the catalyst, we assume this could be due to Nafion present in the catalyst ink which may have overshadowed the nanotubes underneath, making the images inconclusive.

We looked further into this by making another measurement through drop-casting a catalyst ink without Nafion in its formulation. As such, the dispersion of the catalyst was not as good, leaving fewer spots deposited on the substrate. To increase the chances of landing on the catalyst spots during the SECCM experiment and to avoid overlapping of landing spots, we increased the scan area to 100×100 μm^2 with a hopping distance of 3 μm, with 986 (29×34) individual landing spots and a capillary size of ~250 nm. The topography map shows the very flat substrate where the landing points at the studied pixels correspond to different heights, starting from 654 nm, to 721 nm and 1040 nm for spots 1, 2 and 3 respectively, depicted in Figure S8a. Herein, most agglomerates were caught only by one landing point, making the majority of catalyst spots appear as single pixels on the map. These pixels could be counted in the SECCM map and could more precisely be found in SEM by counting the droplet traces, making it more convenient for analysis. The activity map at 0.56 V vs RHE is shown in Figure S8b.

The CVs at different scan rates are presented in Figure S9 while the corresponding R^2 and C_{dl} maps and their values for the spots are shown in Figure S10, Figure 5 and Table S2 respectively. The non-normalized activity map at 0 V vs RHE and the corresponding LSVs in Figure 6a,b show a trend of increasing current from spot 1 to spot 3 (−30 to −300 pA). However, when we normalize the current by the ECSA in

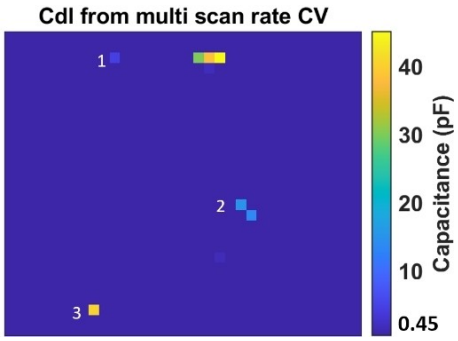

Figure 5. Double layer capacitance C_{dl} acquired from the slope of current vs scan rate.

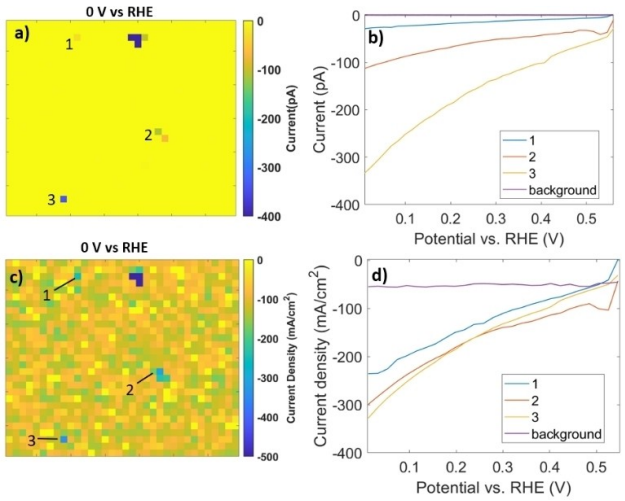

Figure 6. (a) Activity map showing the current in pA at 0 V vs RHE with the investigated agglomerates designated as 1,2,3. (b) LSVs showing the current (pA) vs E vs RHE for the designated pixels in the map. (c) Activity map normalized by ECSA showing the current density in mA cm^{-2} at 0 V vs RHE. (d) Corresponding LSVs for the designated pixels in the normalized activity map, showing current density (mA cm^{-2}) vs E vs RHE. Data correspond to the scan with 100×100 μm^2 area, 3 μm hopping distance, acquired with a ~250 nm pipette filled with 0.05 M H_2SO_4. Catalyst agglomerates do not contain Nafion.

Figure 6c,d, all designated spots level to similar current density values between −225 and −300 mA cm^{-2}, which is interestingly a similar value to the other scan in Figure 4b too, where the catalyst contained Nafion in its formulation. It has been reported in macroelectrode (rotating disc electrode) investigations that the higher content of Nafion leads to an inhibition of ORR due to the blockage of active sites from the Nafion self-assembly.[28] In the nanoscale study, however, such events and the non-electroconductive nature of Nafion did not play a role in the ORR results. Doubtlessly, this is a demonstration of the intrinsic activity of the catalyst where the current is similar independently of Nafion content. The high background current after normalization is explained due to the different C_s of BDD, similarly as before. The activity map normalized considering a C_s of 3 μF cm^{-2} is presented in Figure S11. We analyzed the scanned area with SEM and the image of the full scan is shown in Figure S12, where at these experimental parameters the traces of the meniscus are well separated and there was no flooding occurring. Thereafter, we zoomed into the individual studied spots shown in Figure 7 for a clearer insight into the morphology. Herein one can recognize clearly the presence of nanotubes due to the absence of Nafion in the catalyst. All agglomerates exhibit a mixture of nanotubes and block-like structures, although their ratio seems to be different in the distinct agglomerates. To start with, spot 1 has a morphology dominated by nanotubes, while in spot 2 one can recognize only block-like structures rather than anything else. Moreover, spot 3 exhibits a more clear-cut mixture of the two components, with some nanotubes along with block-like structures. Nevertheless, nanotube or not, the ECSA normalized current densities suggest similar ORR activity in all agglomerates, demonstrating once more the steady ORR activity.

Conclusion

Herein, we investigated individual catalyst agglomerates of a Fe–N-MWCNT catalyst via scanning electrochemical cell microscopy (SECCM). By normalizing the individual electrochemical measurements to their unique ECSA, the intrinsic ORR activity of the catalyst was scrutinized. Similar current densities in different agglomerates were observed, independently of the Nafion content and surface area. Moreover, alike current

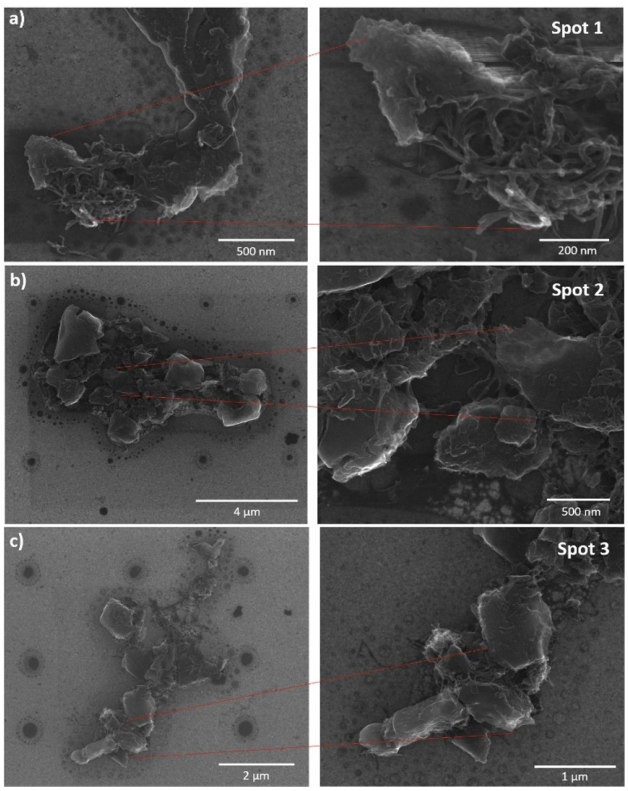

Figure 7. SEM images of (a) spot 1, (b) spot 2, (c) spot 3, corresponding to the traces of SECCM scan with 100×100 μm^2 size, 3 μm hopping distance, ~250 nm pipette filled with 0.05 M H_2SO_4. The catalyst agglomerates herein do not contain Nafion.

densities are obtained for different spots containing variable proportions of nanotubes and block-like structures as investigated with SEM. Overall, the nanomaterial morphology does not seem to be a key parameter influencing the intrinsic ORR activity, which might have crucial implications regarding future synthesis strategies. Nevertheless, further studies of a wider variety of morphologies would be imperative for the generalization of this conclusion.

Experimental Section

SEM measurements

The SEM images were acquired with a Quanta 3D ESEM (FEI) in high-vacuum mode, using an acceleration voltage of 30 kV. Prior to its investigation, the BDD substrate was put onto the aluminum SEM sample holder and contacted with a copper tape to the sample holder which prevents electrostatic charging.

BDD fabrication

Initially diamond nanoparticle (MSY 0–0.03 micron GAF, Microdiamant, Switzerland) seeds were deposited onto a silicon substrate according to a procedure described previously,[29] followed by the growth of a first layer of heavily boron-doped diamond ($[B] = 2 \times 10^{21}$ at.cm^{-3} as determined by SIMS measurements) of approximately 500 nm thickness by microwave-assisted plasma chemical vapor deposition (MPCVD) in a Seki Diamond AX6500 diamond growth reactor in a hydrogen plasma containing 1% methane as the source of carbon and trimethyl boron as dopant. Subsequently, the substrate was transferred to another Seki Diamond AX6500 diamond growth reactor, where a 100 μm thick layer of intrinsic diamond was overgrown onto the BDD layer. Finally, the silicon was removed by wet etching in a mixture of HF/HNO_3 in order to acquire a free-standing diamond film. While the rough surface is the one exposed to the plasma during growth, the smooth surface (boron-doped) is the one originally in contact with the silicon. Since the latter is smooth in the first place, this BDD layer is also smooth (roughness 0.28 nm for a 2 μm area).

Catalyst ink preparation and its deposition

The catalyst powder was synthesized via a procedure described in a previous work.[30] Thereafter, the ink was prepared by dispersing 20 mg of catalyst powder into a 1.175 mL mixture of isopropanol and water (3:1 ratio) and 24 mg Nafion (5% in weight after drying), leading to a concentration of 17 mg mL^{-1}. Subsequently, after adding ~15 g of Zirconium beads, the ink was treated 40 minutes on an IKA ULTRA-TURRAX® Tube Drive for an initial breaking of agglomerates, followed by ball milling for one week in an IKA ROLLER 6 shaker. Thereafter, the beads were removed and the ink was diluted to 0.2 mg mL^{-1}~ and has undergone ultrasonic bath treatment for at least 30 minutes prior to depositing it on the substrate. The same procedure, excluding the Nafion, was followed for the preparation of the catalyst ink without Nafion in it. The flat BDD substrate was rinsed with isopropanol and dried with argon, before fixing it in the holder and contacting it with Cu tape, the conductivity of which was verified with a multimeter. Afterwards, the deposition was done by drop-casting a small drop of the ink on the substrate and letting it dry in the air.

Fabrication of the nanopipette

A CO_2 laser puller (P-2000; Sutter Instruments) was utilized to pull single-barrel quartz capillaries with filament (ZQF-120-90-10; Science Products) through a one-line program, leading to a single barrel pipette. Subsequently, its diameter was determined by SEM (FEI, Quanta 3D ESEM). The pulling parameters utilized for certain capillary sizes are shown below and gave very reproducible results:

(d ~ 150 nm): HEAT 720, FIL 4, VEL 45, DEL 130, PUL 90

(d ~ 250 nm): HEAT 680, FIL 4, VEL 45, DEL 130, PUL 90

SECCM experiment

A home-built SECCM set-up was utilized for the electrochemical experiments, which was installed in a Faraday cage with thermal isolation panels (Vaku-Isotherm) and set on a vibrating damping table (RS 2000, Newport) with four S-2000 stabilizers (Newport). The pipette was filled with 0.05 M H_2SO_4 (99.999% purity, Sigma Aldrich) with a Ag/AgCl [3 M KCl] reference counter electrode inside and was fixed on a pipette holder. The BDD substrate was fixed on top of an x, y, z-piezo cube (P-611.3S nanocube; Physik Instrumente) where an analog amplifier (E-664, Physik Instrumente) aids for fine positioning. An optical camera (DMK 21AU04; The Imaging Source) and a cold light source (KL1500 LCD Schott) were used for visualization by eye while the substrate was initially positioned close to a region of interest, through a three-stepper motor-driven micrometer screws (Owis) with an L Step PCIe (Lang) controller. Once the pipette was ~40 μm above the sample region of interest (working electrode, WE), the approach of the SECCM probe to the WE was done with a surface current (i_{surf}) threshold of 2.5 pA, in order for the contact of meniscus-WE to be detected and further translation to be terminated. The hopping mode protocol was employed for collecting electrochemical data at multiple points, within the restricted area established by the meniscus between the pipette and the substrate. The number of landing points was predefined prior to the experiment. Once the meniscus is in contact with the WE, a linear sweep voltammogram (LSV) in a range of 0.3 to −0.6 V vs Ag/AgCl [3 M KCl] was performed, followed by three cyclic voltammograms (CV) in a range of 0.65–0.7 V vs Ag/AgCl [3 M KCl] at scan rates of 2, 5 and 10 V/s, at each landing spot. The potentials were converted to reversible hydrogen electrode (RHE) via Equation 1, where the standard electrode potential for Ag/AgCl ($E^{o}_{(Ag/AgCl\,[3M\,KCl])}$) = 0.210 V and pH = 1.

$$E_{(RHE)} = E_{(Ag/AgCl)} + 0.059\ pH + E^{o}_{(Ag/AgCl)} \quad (1)$$

While the LSVs were translated to spatially-resolved voltammetric image containing information about the activity of the sample, the CVs at a non-faradaic region were used to calculate the double-layer capacitance. The z-position of approaches at all landing spots was translated to a topography map of the sample. The i_{surf} flowing through the QRCE was determined through a variable gain transimpedance amplifier (DLPCA-200, FEMTO Messtechnik). An FPGA card (PCIe-7852R) served for data acquisition and instrumental control. This was managed through a modified version of software developed at University of Warwick (WEC-SPM) written in LabVIEW (National Instruments).

Data processing

Matlab R2022a (Mathworks) software package was utilized to process all the raw electrochemical data and topography maps. The presented LSVs in the results and discussion section have been smoothed by averaging with 15 adjacent points.

Acknowledgements

The authors acknowledge the SENTINEL project funded by Marie Skłodowska-Curie MSCA-ITN Single-Entity Nanoelectrochemistry under the grant agreement no. 812398.

Conflict of Interest

The authors declare no conflict of interest.

Data Availability Statement

The data that support the findings of this study are available from the corresponding author upon reasonable request.

Keywords: intrinsic activity · multi-walled carbon nanotubes · oxygen reduction reaction · scanning electrochemical cell microscopy · scanning electron microscopy

[1] P. Chandran, A. Ghosh, S. Ramaprabhu, *Sci. Rep.* **2018**, *8*, 3591.
[2] G. J. Offer, D. Howey, M. Contestabile, R. Clague, N. P. Brandon, *Energy Policy* **2010**, *38*, 24–29.
[3] K. Gong, F. Du, Z. Xia, M. Durstock, L. Dai, *Science* **2009**, *323*, 760–764.
[4] Y. Garsany, J. Ge, J. St-Pierre, R. Rocheleau, K. E. Swider-Lyons, *J. Electrochem. Soc.* **2014**, *161*, F628–F640.
[5] I. Dumitrescu, P. R. Unwin, J. V. Macpherson, *Chem. Commun.* **2009**, 6886.
[6] N. Limani, A. Boudet, N. Blanchard, B. Jousselme, R. Cornut, *Chem. Sci.* **2021**, *12*, 71–98.
[7] Y. Takahashi, A. Kumatani, H. Shiku, T. Matsue, *Anal. Chem.* **2017**, *89*, 342–357.
[8] P. Bertoncello, *Energy Environ. Sci.* **2010**, *3*, 1620.
[9] A. J. Bard, M. V. Mirkin, Eds., *Scanning Electrochemical Microscopy*, CRC Press, Boca Raton, Fla, **2012**.
[10] C. G. Zoski, *J. Electrochem. Soc.* **2016**, *163*, H3088–H3100.
[11] K. Eckhard, X. Chen, F. Turcu, W. Schuhmann, *Phys. Chem. Chem. Phys.* **2006**, *8*, 5359.
[12] V. Singh, A. Tiwari, T. C. Nagaiah, *J. Mater. Chem. A* **2018**, *6*, 22545–22554.
[13] A. Tiwari, V. Singh, T. C. Nagaiah, *J. Mater. Chem. A* **2018**, *6*, 2681–2692.
[14] N. Ebejer, M. Schnippering, A. W. Colburn, M. A. Edwards, P. R. Unwin, *Anal. Chem.* **2010**, *82*, 9141–9145.
[15] C. L. Bentley, M. Kang, P. R. Unwin, *Curr. Opin. Electrochem.* **2017**, *6*, 23–30.
[16] N. Ebejer, A. G. Güell, S. C. S. Lai, K. McKelvey, M. E. Snowden, P. R. Unwin, *Annu. Rev. Anal. Chem.* **2013**, *6*, 329–351.
[17] P. R. Unwin, A. G. Güell, G. Zhang, *Acc. Chem. Res.* **2016**, *49*, 2041–2048.
[18] C.-H. Chen, K. E. Meadows, A. Cuharuc, S. C. S. Lai, P. R. Unwin, *Phys. Chem. Chem. Phys.* **2014**, *16*, 18545.
[19] M. Choi, N. P. Siepser, S. Jeong, Y. Wang, G. Jagdale, X. Ye, L. A. Baker, *Nano Lett.* **2020**, *20*, 1233–1239.
[20] E. B. Tetteh, L. Banko, O. A. Krysiak, T. Löffler, B. Xiao, S. Varhade, S. Schumacher, A. Savan, C. Andronescu, A. Ludwig, W. Schuhmann, *Electrochem. Sci. Adv.* **2022**, *2*, e2100105.
[21] J. C. Byers, A. G. Güell, P. R. Unwin, *J. Am. Chem. Soc.* **2014**, *136*, 11252–11255.
[22] R. G. Mariano, O. J. Wahab, J. A. Rabinowitz, J. Oppenheim, T. Chen, P. R. Unwin, M. Dincă˘, *ACS Cent. Sci.* **2022**, *8*, 975–982.
[23] O. Henrotte, A. Boudet, N. Limani, P. Bergonzo, B. Zribi, E. Scorsone, B. Jousselme, R. Cornut, *ChemElectroChem* **2020**, *7*, 4633–4640.
[24] C. L. Bentley, R. Agoston, B. Tao, M. Walker, X. Xu, A. P. O'Mullane, P. R. Unwin, *ACS Appl. Mater. Interfaces* **2020**, *12*, 44307–44316.
[25] N. I. T. Ramli, S. Abdul Rashid, Y. Sulaiman, M. S. Mamat, S. A. Mohd Zobir, S. Krishnan, *J. Power Sources* **2016**, *328*, 195–202.
[26] C. L. Bentley, *Electrochem. Sci. Adv.* **2022**, *2*, e2100081.
[27] A. Fujishima, Y. Einaga, T. N. Rao, D. A. Tryk, *Diamond Electrochemistry*, Elsevier Science, Burlington, **2005**.
[28] J. Chlistunoff, J.-M. Sansiñena, *J. Electroanal. Chem.* **2016**, *780*, 134–146.
[29] H. A. Girard, E. Scorsone, S. Saada, C. Gesset, J. C. Arnault, S. Perruchas, L. Rousseau, S. David, V. Pichot, D. Spitzer, P. Bergonzo, *Diamond Relat. Mater.* **2012**, *23*, 83–87.
[30] A. Boudet, O. Henrotte, N. Limani, F. El Orf, F. Oswald, B. Jousselme, R. Cornut, *Anal. Chem.* **2022**, *94*, 1697–1704.

Manuscript received: November 14, 2022
Revised manuscript received: January 5, 2023